Journal of Himalayan Earth Sciences Volume 56, No. 1, 2023 pp. 48-64

A Source Model for Tsunami Hazards. A Case study from the Eastern Segment of the Makran Subduction Zone, Balochistan, Pakistan

Babar Ali[1]*, Ryo Matsumaru[2] and Hammad Tariq Janjuhah[3]

[1]Graduate School of Global and Regional Studies, Toyo University Tokyo, Japan.

[2]Faculty of Global and Regional Studies, Toyo University, Tokyo, Japan.

[3]Department of Geology, Shaheed Benazir Bhutto University, Sheringal, Dir (U), KP, 18050, Pakistan.

**Corresponding author: babarpmd@gmail.com*

Submitted date: 18/11/2022 Accepted date: 06/04/2023 Published online: 17/04/2023

Abstract

Population growth and economic development on the Pakistani coasts necessitate tsunami hazard analyses. Numerous valuable research outputs already exist given the 1945 Makran earthquake and tsunami. To fill the gap, and present additional scenarios regarding the characteristics of tsunamis at these coasts, an innovative tsunami source model is developed for simulations. The geographical information system (GIS) techniques are used for the mapping of seismogenic sources, placing the fault planes and approximation of their extent in the source model. The segmentation of the Makran subduction zone is practiced, designating its eastern segment as a tsunami source region. The extent of rupture induced by the 1945 Makran earthquake is related to the size of the tsunami source in the formulation of the new source model. The earthquake catalogs and literature on previously developed source models are consulted to estimate various constituting parameters of this model. The bathymetry profile near coasts is analyzed to assess the susceptibility of submarine landslides that may enhance tsunami impacts. Simulations of the 1945 tsunami yielded ~5 m high wave while simulation of the worst tsunami based on an Mw 8.6 earthquake scenario yielded an amplitude of ~8 m. The late and prolonged arrival of high waves after the first tsunami is also observed in simulations.

Keywords: Makran subduction zone, tsunami, numerical simulation, deterministic tsunami hazard analysis.

1. Introduction

The tsunami risk on the coasts of Pakistan is increasing over time due to unsustainable urbanization and population growth. The Pakistan Meteorological Department maintains a database of historical earthquakes showing a record of two tsunamigenic earthquakes in 1851 AD and 1864 AD. On the Modified Mercalli Intensity scale, their intensity was VII at Gwadar. According to Rastogi and Jaiswal (2006), the coasts of Pakistan were hit by tsunamis in 326 BC, 1008 AD, and 1945 AD. Moreover, historical evidence of more than a few tsunamis are presented by Heidarzadeh et al. (2008) that impacted these coasts. This historical information suggests that tsunamis are inevitable in the future as well.

The epicenter of the off-coast Makran earthquake (28th November 1945) was in the Makran subduction zone (MSZ). It caused a tsunami that took 4,000 lives (Pararas-Carayannis, 2006). According to the studies on the probabilistic seismic hazard analysis (PSHA) conducted by Asad et al. (2021) and Ahmed et al. (2022), the likelihood of a large earthquake in the MSZ (that has the potential to trigger tsunamis) in the future is inevitable and necessitates the deterministic tsunami hazard analysis (DTHA).

The DTHA focuses on modeling the specific physical characteristics of a single, worst-case scenario tsunami (Tinti & Armigliato, 2003 and Tinti et al., 2005). This method uses numerical models to simulate the physical processes that occur during a tsunami, such as the propagation of waves and their interaction with coastal features (Lovholt et al., 2006 and Lorito et al., 2008). The DTHA assumes specific earthquake magnitude and location while using a numerical model to predict the tsunami's propagation, arrival time, and maximum wave height at various coastal locations comprehensively (Harbitz et al., 2012 and Omira et al., 2013). The probability associated with different earthquake scenarios or the uncertainty is not accounted for by the DTHA.

We identified the tsunami source region, formulated a tsunami source model, and conducted scenario-based numerical simulations viz. The 1945 tsunami and that from the largest possible earthquake in the MSZ. The amplitude (or wave heights) of the tsunami and its time of arrival are recorded by nine virtual tide gauges near the coasts.

Several researchers studied the formulation of novel source models for the MSZ. The alteration or adjustment in the constituting parameters gives an innovative source model, thereby suggesting plentiful options. In this regard, the research of Heidarzadeh et al. (2008) and that of Heidarzadeh et al. (2009) can be considered as pioneering work. Another prominent precedential study is conducted by Jaiswal et al. (2009) on tsunami source modeling. Neetu et al. (2011) put forward some significant aspects of the hypothesis of the 1945 tsunami. Further contributions in modernizing the understanding of this tsunami are delivered by Heidarzadeh and Satake (2015). It is worthwhile mentioning the work of Rehman et al. (2015). They used six larger fault planes as source areas in their tsunami simulations. Zuhair and Alam (2017) examined the tsunami vulnerability to nuclear power plants focusing on the western coasts of India. Rastgoftar and Soltanpour (2016) identified the submarine landslide location that was triggered due to the 1945 Makran earthquake.

The review of precedential work revealed various shortcomings including the discrepancy in the positioning and alignment of the tsunami source region or the fault planes. We developed the New Tsunami Source Model (New-TSM) to address the deficiencies including inconsistency in the alignment of the MSZ concerning the source area's strike angle, and negligence in the subdivision of the MSZ. Hence, a considerable portion of this paper covers justification and explanation about the selection of the New-TSM constituents.

The geographical information system (GIS) techniques are employed for mapping seismogenic zones that can generate tsunamigenic earthquakes and for plotting their seismicity. The bathymetry profile at the steep continental slope is analyzed to examine the likelihood of a submarine landslide that can trigger a tsunami. The length and width of rupture induced by the 1945 earthquake are used as the extent of the tsunami source (the area of fault planes) in numerical simulations for the first time in this study. We performed the comparison between simulation results obtained from the novel source model developed in this study and those yielded by the model developed by Heidarzadeh and Satake (2015) (also referred to as H&S-15). The magnitude of the largest possible earthquake that the eastern MSZ can generate. This scenario is evaluated to predict the worst tsunami scenario.

2. Geology and Tectonics Near Pakistani Coasts

The coasts of Pakistan are divided into two geomorphic sections. The eastern and the western section. The western section comprises rocky cliffs while the eastern section has low flat delta plains. The present situation of vulnerability to tsunamis is greatly related to this geomorphic division of the topography. Solangi et al., (2019) are of the view that the eastern section corresponds to the Indus offshore basin beneath the Arabian Sea, whereas the western section of Pakistani coasts is parallel to the offshore basin in the vicinity of Makran. The geological and tectonic maps from some prestigious research work (for instance, Kukowski et al., 2000 and Burg, 2018) are georeferenced. Bird (2003) and HCP (2008) prepared shapefiles of tectonic plate boundaries. We overlaid these shapefiles on the georeferenced tectonic maps for mapping various fault lines and analysis of seismicity on a regional scale, as shown in Fig. 1.

2.1 Eastern Section

A large part of Sindh province and a minor part of Balochistan province is covered by the 'lower Indus platform basin'. Its northern and western boundaries are marked by the Sulaiman Ranges and the Kirthar Ranges, respectively. The eastern section of Pakistani

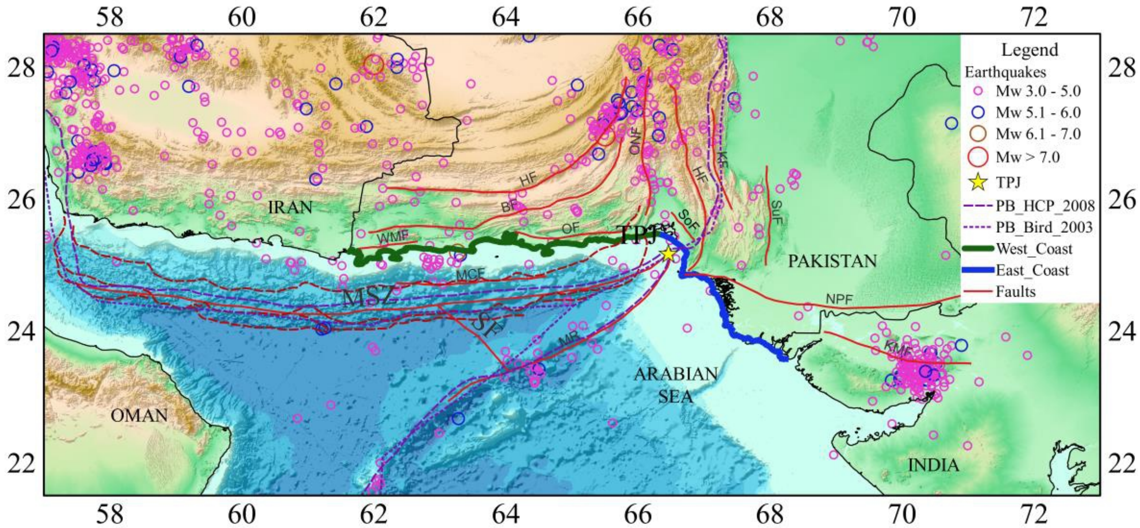

Fig. 1. Seismicity data source USGS; PB is the short form of 'plate boundaries' proposed by HCP (2008) and Bird (2003); TPJ represents the triple plate junction of three tectonic plates.

coasts lies in the south of this basin (Kazmi & Jan, 1997). Its total length is ~350 km. While measuring the length of this section, we excluded the tidal channels and creeks. The blue curve in Fig. 1 represents the Indus River which forms the low flat delta plains. These plains cover the coastal areas from Sir Creek (situated near the Indian border) to Sonmiani (situated in the west of Karachi). Snead (1966) indicated some white sandy beaches within the ~80 km section between Gaddani and Karachi. Vast inland areas of these coasts are low-lying and can be inundated by tsunamis.

The notable seismogenic zones near the eastern section of the Pakistani coasts are Kutch Mainland fault (KMF), Nagar Parker fault (NPF), Surjan fault (SuF), Kirthar fault (KF), Pub fault (PF), Sonmiani fault (SoF), and Murray Ridge (MR). On the western section of the coasts, some of the most prominent faults are Buzadar fault (BF), Ormara fault (OF), Ornach Nal fault (ONF), Hoshab fault (HF), Sonne fault (SF), West Makran fault (WMF), Makran Coast fault (MCF), and Makran Subduction Zone (MSZ) (Fig. 1).

2.2 Western Section

A repetitive series of extremely folded and faulted mountain ridges and valleys exist near the western section of Pakistani coasts. These are called the Makran Ranges. According to Kazmi and Jan (1997), these ranges cover 400 × 250 km2 area. The tertiary volcanic rocks are the main constituents of the Makran Ranges (Farhoudi and Karig, 1977). The western coast is elevated due to these ranges and headlands (Khan, 1999). These terraces and raised beaches can protect the inland population from tsunamis. In the south, the borderline of the Makran fold-belt basin coincides with the Pakistani coasts. In the west, the end-point is at Jiwani (situated near the Iranian border) whereas the eastern end-point is at Sonmiani. It covers a larger part of the entire coastline, as indicated in Fig. 1.

2.3 Makran Subduction Zone

The MSZ is an east-west striking shallow active continental margin situated near the coasts of Pakistan and southeastern Iran, where the oceanic floor of the Arabian tectonic plate subducts under the Eurasian tectonic plate (Farhoudi & Karig, 1977). Quittmeyer & Jacob (1979) recognize it as a tectonic system comprising faults and lineaments. The Zendan-Minab fault system marks the western terminus of the MSZ while its eastern terminus is at the intersection of the Murray ridge and the Ornach Nal fault (Heidarzadeh et al., 2008). The epicenter of the 1945 tsunamigenic earthquake lies on the MSZ. The approximate length of this zone is ~1000 km (Byrne et al., 1992). Considering this characteristic, the MSZ should be considered as a possible source of future tsunamigenic earthquakes.

3. Methodology

The objective of formulating the New TSM is to regenerate the 1945 tsunami and to predict the worst tsunami scenario. The earthquake parameters from the centroid moment tensor (CMT) solutions can function as the tsunami source model. The insufficiency of such data in the MSZ hinders the formulation of a reliable source model. The initial conditions of the tsunami can be calculated by using tide gauge data (e.g. the method used by Lay et al., 2005). Various types of tide gauge data of the 1945 tsunami, including the travel time and amplitude, are also inadequate. The first mapping survey was reported in 1947 by Heck (1947). Another survey was conducted 34 years after the tsunami by Page et al. (1979). Shah-Hosseini et al., (2011) indicate that the researchers worked on the 1945 tsunami even 66 years later. Furthermore, two surveys after 68 years of this tsunami are conducted by Hoffmann et al. (2013) and another by Kakar et al. (2013). The latest documented survey is done by Okal (2015). A lot of useful information about tsunami travel time and amplitude at the coasts is lost as surveys were not performed right after the tsunami. Presently, simulation of the 1945 tsunami is an uphill task to be performed by using any of the aforementioned methods. Therefore, to overcome this difficult situation, we derived the New-TSM relying on the geological features related to the MSZ.

3.1 Positioning the Tsunami Source Area

The fault planes (FPs) are two-dimensional flat surfaces. On two-dimensional maps, the FPs show a rectangular projection. In numerical simulations, these are regarded as the tsunami source area. The location, area, depth, strike, dip, rake, and co-seismic slip along the FPs, control tsunami propagation and amplitude in simulations. Their area and dislocation are also used in the calculation of Mw. Therefore, the appropriateness of these parameters is imperative in the formulation of the New-TSM.

Some of the most notable faults situated near the coasts are Kutch Mainland Fault, Nagar Parker Fault, Surjan Fault, Kirthar Fault, Pub Fault, Sonmiani Fault, Murray Ridge, Buzadar Fault, Ormara Fault, Ornach Nal Fault, Hoshab Fault, Sonne fault, West Makran fault, Makran Coast fault, and Makran Subduction Zone. It is evident from the literature that the Buzadar fault (BF) and the MSZ can produce tsunamigenic earthquakes. A record of only one tsunamigenic earthquake of Mw 7.7 on September 24, 2013, is found near the BF. The documented impacts of this tsunami are negligible as compared to those induced by the 1945 tsunami. The historical evidence attributes all the tsunamigenic earthquakes in the vicinity of Pakistani coasts to the MSZ. Therefore, this zone is considered a major tsunamigenic source and the backbone of developing the New-TSM. We hypothesized that the source area for all simulations in this study has to be the MSZ. As the New-TSM is developed explicitly for the MSZ; thereby its location, segmentation, and strike angle (θ) play an important role in positioning the FPs. The placement of the FPs, their θ, and their area are calculated by overlaying the geological maps of the MSZ on the boundaries of three tectonic plates. This process is completed by using an open-source utility called the QGIS (version 3.20.2). The results from some overlaid maps are shown in Fig. 2. The plate boundaries coincide with the MSZ which is put forward by Kukowski et al. (2001). The green curves represent some lineaments of the MSZ, as proposed by Quittmeyer and Jacob (1979) and outlined by Burg (2018). The green curves indicate a relatively broader depiction of the MSZ as these curves envelop the Arabian, Eurasian and Indian plate boundaries and other proposed locations of the MSZ. These features of the MSZ (green curves) proposed by Burg (2018) are adequately considerable to accept its location for positioning the FPs. Moreover, their area and θ are evaluated from the base map of Burg (2018).

3.2 Segmentation of the MSZ

The Sonne fault divides the MSZ at 24.4°N and 62.9°E (Musson, 2009) into two parts termed the eastern and western segments of the MSZ. According to Hussain et al. (2002) the TPJ is located in the south of Sonmiani (Fig. 2). The aforementioned point of intersection and the TPJ encompass the eastern segment of

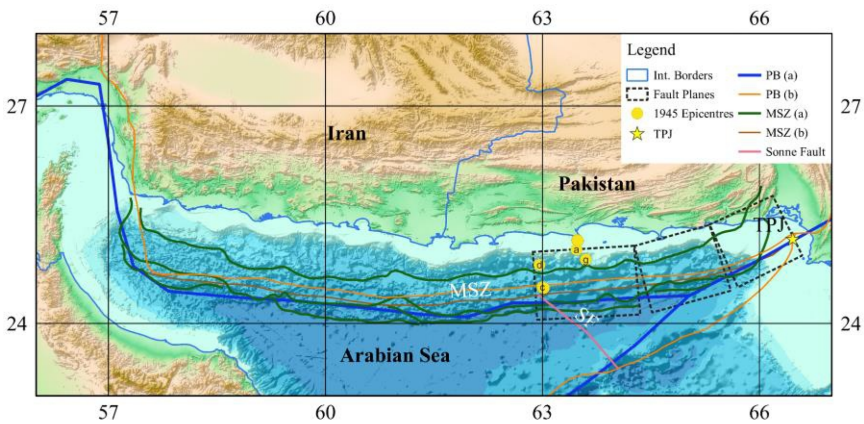

Fig. 2. Tectonic plate boundaries (PB) along with the MSZ from various geological maps. Source of the plate boundaries: Bird (2003) and HCP (2008). Source of MSZ: Burg (2018). SF stands for Sonne fault (source: Kukowski et al., 2001). TPJ stands for the triple plate junction.

the MSZ. The estimated length of the eastern MSZ is 350 to 400 km (Pararas-Carayannis, 2006) while that measured (using QGIS in this study) is ~380 km. Musson (2009) is of the view that the earthquake generated by any of these segments (regardless of its magnitude) would not induce a rupture in the other segment.

The historical earthquakes are largely centered on the eastern segment of the MSZ (for instance, Heiderzaheh et al., 2008 and Byrne et al., 1992). An intermediate to low seismicity is also indicated by these historical data except for a few large magnitude earthquakes, e.g., the tsunamigenic earthquake in 1945. The high seismicity is justified by the higher convergence rate of tectonic plates on the eastern segment (Rajendran et al., 2012). These arguments establish that the eastern segment has more potential to generate tsunamis as compared to the western segment. At this stage, it is worthwhile mentioning that Pakistani coasts are nearer to the eastern segment while Iranian coasts are situated in the proximity of the western segment. Consequently, the eastern segment poses a larger risk of tsunami toward the coastal areas of Pakistan. This study aims to conduct the DTHA for Pakistani coasts; thus, the eastern segment is selected as the source region for the New-TSM. The θ of the MSZ does not vary along its western segment but it varies continuously along the eastern segment. Therefore, tsunami simulations with only one FP or several FPs with uniform strike angel can give errors in arrival times and amplitudes. The issue is fixed by dividing the source region into three FPs having θ = 243°, 254° and 266° (from east to west), aligned with the strike angle of the eastern MSZ, as observed in Fig. 2. The θ is approximated (using a function in QGIS software) from the tectonic maps obtained from Kukowski et al. (2000) and Burg (2018).

3.3 Earthquake Magnitude

The magnitude of the 1945 earthquake on the Richter scale calculated by the seismic station Quetta was less than 6.7 (Snead, 1966). The epicenter of this earthquake was 400 km away from this station, where a drum-type photographic seismometer is installed (author's personal). The distance between the seismic station and the epicenter, and the instrument error are likely to cause an error in the calculation of the magnitude. The surface wave magnitude (Ms) and the seismic moment calculated by Pacheco and Sykes (1992) are 8.0 and 10.2 × 1027 dyne·cm, respectively. The seismic moment of this earthquake is between 7.5 × 1027 and 8.0 × 1027 dyne·cm (Quittmeyer and Jacob, 1979) which is approximately equal to Mw 7.9. Byrne et al. (1992) argue that the moment magnitude is 8.0 – 8.24. Previously, Gutenberg and Richter (1954) calculated Mw 8.25 for the Makran earthquake. In pursuance of these estimations, we used Mw 8.2 for the simulation of the 1945 tsunami.

The tsunami simulations largely depend on the Mw of the earthquake. The moment magnitude can be calculated by equations relating several fault parameters. We used the equation proposed by Hanks and Kanamori (1979), given as:

$$M_w = 0.667 \log_{10}(M_o) - 10.7 \qquad (1)$$

In this equation, the seismic moment is represented by M_o. Aki (1966) defined it as a product of the shear modulus of the earth, area of the fault planes, and the dislocation along the fault planes. Its mathematical form is:

$$M_o = \mu \times \text{area} \times \Delta u, (2)$$

where, the shear modulus is equal to 3.0×10^{10} $N \cdot m^{-2}$ for the MSZ (Bonilla et al., 1984).

The 1945 Makran earthquake induced a rupture along the MSZ. The rupture length is between 150 and 200 km whereas its width is 40 km (Quittmeyer and Jacob, 1979; Jaiswal *et al.*, 2009). We set the rupture area as a standard and consulted the maps of the MSZ from Kukowski *et al.* (2000) and Burg (2018) to approximate length and width of the FPs. The proposed lengths of the FPs (oriented: east-west) are 40 km, 65 km, and 90 km. Table 1 provides a comparison of the size of the FPs from previous studies with the rupture area of the 1945 earthquake.

The co-seismic slip (Δu) along the MSZ due to the 1945 Makran earthquake is 6 to 8 m (Byrne *et al.*, 1992). However, earlier in their simulations, Heidarzadeh *et al.* (2008) fixed the Δu to 7.3 m, whereas Neetu *et al.* (2011) fixed it to 7.0 m. In another study, Zuhair and Alam (2017) suggested $\Delta u = 11$ m. On the other hand, Jaiswal *et al.* (2009) increased the co-seismic slip to 15 m. We applied the trial and error method in Eq. (1). The value of Δu is varied while M_w and the area are kept constant. In this way, the co-seismic slip (or dislocation) comes out to be 11 m.

The three FPs of the New-TSM can produce $M_o = 2.57 \times 10^{28}$ dyne·cm, corresponding to M_w 8.2 earthquake from Eq (1) for simulation of the 1945 tsunami. The largest hypothetical earthquake the eastern MSZ can produce is estimated to simulate the worst tsunami scenario. For doing so, the area of the FPs is repeatedly increased in Eq (1) keeping the dislocation constant at 11 m. Also, the tsunami source area is kept within the bounds of the eastern MSZ during this process. The estimated area of the eastern segment of the MSZ is 33,750 km^2 (from the tectonic map of Burg, 2018). We considered this as the maximum size of the FPs for the eastern MSZ. With this area, the FPs can produce $M_o = 1.01 \times 10^{29}$ dyne·cm corresponding to M_w 8.6. We pronounced this as the maximum credible earthquake for the eastern MSZ. Hence, the M_w 8.6 earthquake scenario is attained by increasing the area of the FPs step-by-step without altering other parameters of the New-TSM.

3.4 Dip and Rake

The dip and rake of the fault planes (mostly represented by δ and λ) can be evaluated from the focal mechanism or the CMT solutions; however, the scarcity of such data for the MSZ imposes a major hindrance. We consulted the available scientific literature on the tectonic framework and previous work on tsunami simulations to estimate dip and rake. According to Heidarzadeh *et al.* (2008), the MSZ dips at a shallow subduction angle having a value from 2° to 8°. However, Okal's *et al.* (2015) calculation gave $\delta = 9°$. The seismic waveform data analyzed by Byrne *et al.* (1992) from earthquakes the MSZ, suggests 7° for its dip. Also, Heidarzadeh and Satake (2015) and Zuhair and Alam (2017) set $\delta = 7°$ for this zone. We selected the earthquakes lying within the FPs from the GCMT catalog and calculated the average value of δ which came out to be 7°. Therefore, the same is assigned to each of the three Fps.

As far as the rake is concerned, Byrne *et al.* (1992) suggest 89° for the MSZ. Their suggestion is agreed upon by Okal *et al.* (2015). The same value is opted for by Heidarzadeh and Satake (2015) whereas, Zuhair and Alam (2017) opted for 90°. We adopted 89° for each of the fault planes.

3.5 Depth of the Fps

The depth distribution of seismicity near the eastern MSZ is analyzed. For this purpose, three catalogs including GCMT, EMSC, and USGS are used. Due to fewer records of an earthquake found in this area in the GCMT and EMSC catalogs (*i.e*., eight and 38 earthquakes, respectively), no decisive results can be drawn, as shown in Fig 3 (*a*). The USGS catalog contained 417 earthquakes for the entire MSZ having an average focal depth of 20.09 km.

To produce a more reliable depth versus magnitude profile, we considered a smaller spatial window that only focused on the fault planes. Thus, reducing the number of earthquakes to 100. Their depth versus magnitude profile is shown in Fig 3 (*b*). The focal depth is 20.45 km (averaged).

According to Jackson and McKenzie (1984), generally shallow earthquakes occur in the MSZ. Later this claim is supported by Byrne *et al.* (1992) and Satake & Tanioka (1999). Referring to the analysis of the depth versus magnitude profile and the earlier findings, a focal depth equal to 20.45 km is assigned to the fault planes in our novel tsunami source model.

3.6 Submarine Landslide

A run-up of 4 to 5 m is found by Heidarzadeh *et al.* (2008) in the simulation of the 1945 tsunami. On the other hand, tsunami amplitudes of 12 to 15 m are reported by Berninghausen (1966) and Snead (1966). In this regard, Bilham *et al.* (2007) explained that a submarine landslide caused by the Makran earthquake increased the wave height. Rajendran *et al.* (2008) supported this viewpoint.

Pasni and Ormara (on the western section of the coast) were confounded by more than a few tsunami waves due to the landslide. Their persistent arrivals continued hours after the main shock (Ambraseys and Melville, 1982). The corroboration concerning the occurrence of a landslide that followed the 1945 earthquake is pioneered by Rastgoftar and Soltanpour (2016). Later, Heiderzadeh and Satake (2017) suggested a few more innovations. Both of these studies marked the location of a submarine landslide near Ormara and Pasni. These are represented by small red squares in Fig 4 (*a*) on the continental slope. The lines culminating at points labeled 'RS' (Rastgoftar and Soltanpour shortened) and 'HS' (Heiderzadeh and Satake shortened) pass through these locations. A line passing through the 'offshore Indus basin' terminates at 'IR' (short form for the Indus River). To examine the likelihood of submarine landslides, we analyzed the bathymetry profile along 12 lines, presented in Fig. 4(*a*). Their endpoints are the deepest parts of the Arabian Sea nearest to the coast (1 km to 2.5 km away). The data of 15 arc-seconds resolution from the GEBCO (BODC, 1997) is used for this analysis. The bathymetry profiles off the coasts are shown in Fig. 4 (*b*), (*c*), and (*d*).

The fan-shaped 'offshore Indus basin' lies near the eastern section of Pakistani coasts. Its main constituents of this basin are sand and shale which are deposited on the steep continental slope by the Indus River (Solangi *et al.*, 2019; Khan, 1999). The bathymetry profiles in Fig. 4 (*c*) and Fig. 4 (*d*) reveal a few sites along this basin where the slope becomes steeper than the western coast (the landslide sites) as shown in Fig. 4(*b*), hence making it evident that the susceptibility to submarine landslides has uniform distribution along all continental slopes. So far, the lack of such events is probably due to the absence of large earthquakes off the eastern coast.

The tsunami impact depends on the energy released by the earthquake. Submarine landslides can cascade the tsunami impact. The question: “if the effect of this landslide is added in the results of Heidarzadeh *et al.* (2008), would it result in 12 to 15 m tsunami amplitudes”, remains unanswered. Neetu *et al.* (2011) opposed the idea of amplified waves arriving hours after the first tsunami as a result of a submarine landslide. They explained that the tsunami waves which propagated on the continental shelf got trapped and reflected back and forth. These reverberations of the tsunami waves repeatedly hit the coasts. The width of the continental shelf is not uniform which is another reason for this continuous attack of tsunami waves. These reasons are convincingly sufficient not to consider the submarine landslides in the formulation of the New-TSM.

Table 1. The area of the rupture induced by the 1945 earthquake is compared with the area of the fault planes from various studies.

Study	Length (km)	Width (km)	FPs	Area (sq. km)
Quittmeyer and Jacob (1979)	150 - 200	40	-	6,000 - 8,000
Neetu *et al.* (2011)	100	100	1	10,000
Heidarzadeh and Satake (2015)	70	55	4	15,400
Rehman *et al.* (2015)	100	50	6	30,000
Zuhair and Alam (2017)	378	180	1	68,040
This study	195	40	3	7,800

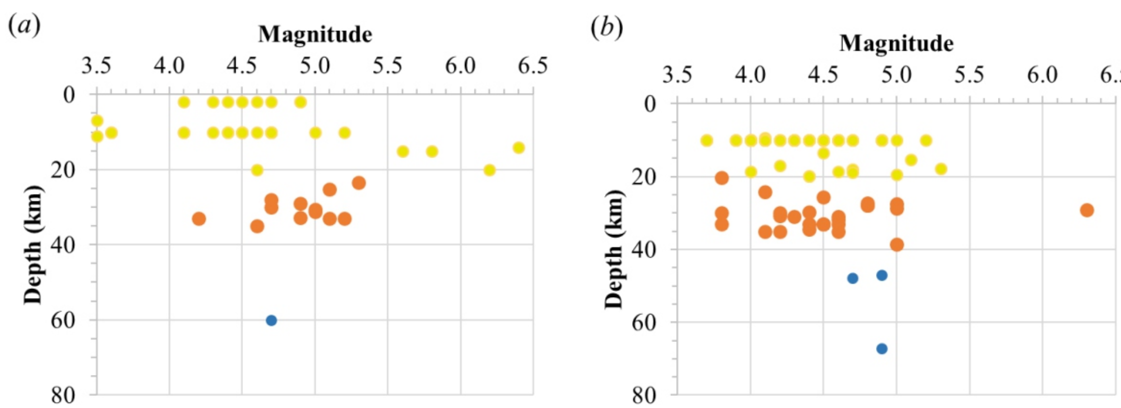

Fig. 3. Depth – magnitude (Mw) profile for the MSZ. (a) EMSC and GCMT catalog; (b). USGS catalog.

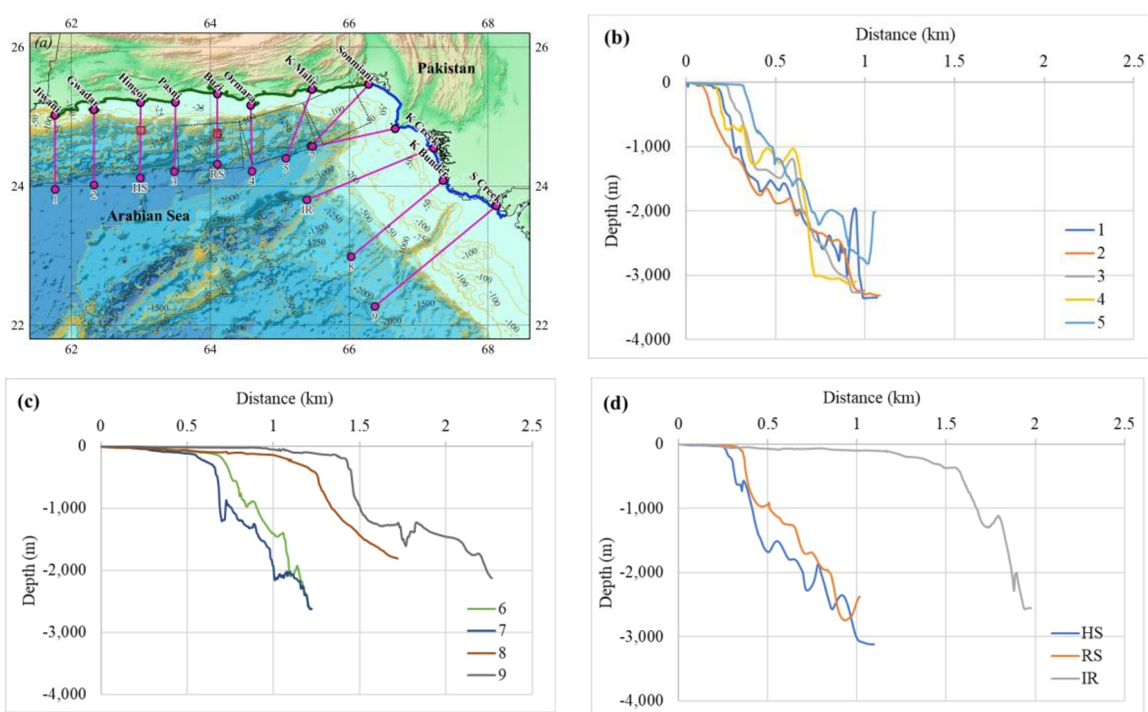

Fig. 4 (a) Bathymetry profile off the coasts of Pakistan is analyzed along the purple lines. FPs are represented by dotted rectangles. (b) The western section of Pakistani coasts. (c) The eastern section of Pakistani coasts. (d) Bathymetry profile of the landslide sites and the Indus basin.

3.7 Advantage of the New-TSM over other Source Models

The dotted curves in cyan indicate various lineaments of the MSZ (as proposed by Burg, 2018) in Fig. 5. The eastern segment of the MSZ lies between the Sonne fault and the TPJ. The single fault plane used by Zuhair and Alam (2017) in their simulations is represented a magenta rectangle that is away from the coast and the MSZ. The FPs by Rehman et al. (2015) do not cover the entire MSZ, nor do they coincide with its eastern segment (five brown rectangles). Expansively larger Mw, as compared with the 1945 Makran earthquake, is resulted from the enormously large fault planes set by Rehman et al. (2015). The same applies to the single-fault plane set by Zuhair and Alam (2017).

Heiderzadeh and Satake (2015) proposed four fault planes. The location and the orientation of these fault planes do not coincide the entire MSZ. The blue rectangles represent the fault planes of the New-TSM. Their location and orientation are concisely in agreement with the eastern segment.

4. Results of Tsunami Simulations

For numerical simulations, we selected 540 grids in the N-S direction (18°N to 27°N latitude) and 720 grids in the E-W direction (57°E to 69°E longitude). Size of each grid is 1,800 m. This computational domain covers all coastal areas of Pakistan. The total duration of each simulation is 5 hours with time step = 1 second. The GEBCO (BODC, 1997) bathymetry data (15 arc-second resolution) is used.

Regarding the initial conditions, it is worthwhile mentioning that the method proposed by Mansinha and Smylie (1971) is used for the estimation vertical component of displacement at the sea bed. This displacement functions as a tsunamigenic earthquake. We used the numerical model developed by Mikami *et al.* (2014) for tsunami simulations. The leap-frog method, which is mostly used in numerical integration to solve differential equations, is employed by the aforementioned model.Nine virtual tide gauges (represented by encircled numerals in Fig. 6) recorded the simulated tsunami arrival times and their amplitudes. The sites for these gauges are selected near prominent coastal towns or cities. The nine gauges are (on average) a hundred kilometers apart corresponding to an idyllic situation for quantification of the DTHA.

4.1 Propagation of the Tsunami

The blue and green rectangles in Fig. 6 denote the FPs for M_w 8.2 earthquake scenario for the New-TSM and H&S-15's source model, respectively. These are used for the simulation of the 1945 tsunami. The red rectangles represent the FPs for M_w 8.6 earthquake scenario for the New-TSM to simulate the worst tsunami for Pakistani coasts. We incorporated the source model for these earthquake scenarios into the numerical model, one by one. The snapshots of the tsunami wavefronts (WFs) are denoted by the curves having the same color as their sources (*i.e.*, the fault planes).

Each time the model is operated, it gave tsunami wave propagation as a separate output. The comparison of propagation and other related characteristics from different source models is difficult in this situation. Therefore, we replicated the original outputs with the help of the QGIS software. These outputs are georeferenced in a single raster layer. Then the wavefront is traced and overlaid on a single GEBCO bathymetry map (Fig. 6).

The snapshots of simulated tsunami wavefronts yielded 20, 40, and 60 minutes in the case of the M_w 8.6 earthquake scenario are represented by the red curves in Fig. 6. It is evident that this tsunami wave propagates faster than the other two generated by the earthquake scenario having magnitude 8.2. The wavefront thirty minutes after the 8.2 magnitude earthquake and that twenty minutes after the 8.6 magnitude earthquake are almost coincident in the deep sea.

The wavefront one hour after the 8.2 magnitude earthquake and forty minutes after the 8.6 magnitude earthquake reached simultaneously at Omani coasts. However, there is a considerable difference in the arrival time of tsunamis on the eastern section of Pakistani coasts and the adjoining Indian coasts, as shown in Fig. 6.

4.2 Tsunami Waveforms

The tsunami waveforms yielded from the New-TSM for the 8.2 magnitude earthquake scenario is represented by blue curves whereas those for the 8.6 magnitude earthquake scenario are represented by red curves in Fig. 7. The waveforms for the 8.2 magnitude earthquake scenario from the H&S-15 are represented by the green curves. The wave height of the simulated tsunami amplified and the arrival time decreased, as the earthquake magnitude increased from 8.2 to 8.6 as shown in Fig. 7.

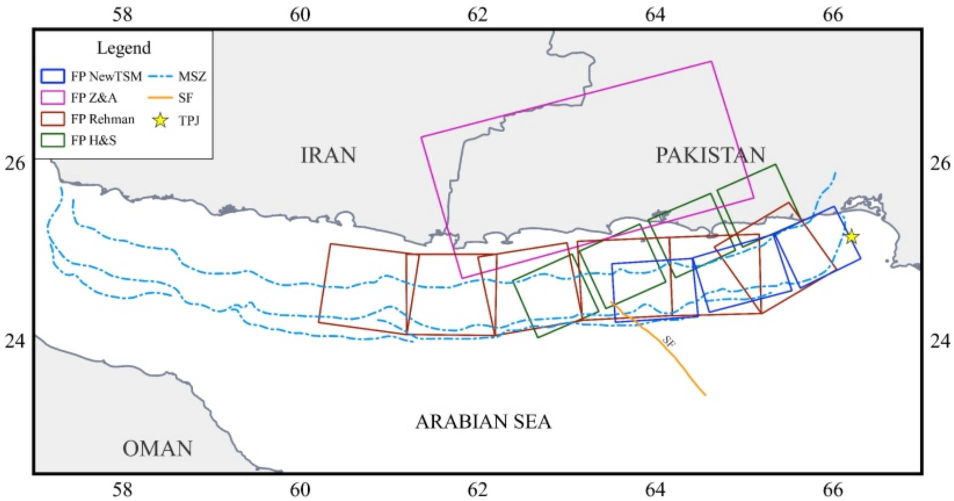

Fig. 5. Comparison of the FPs from the New-TSM with those from the previous studies.

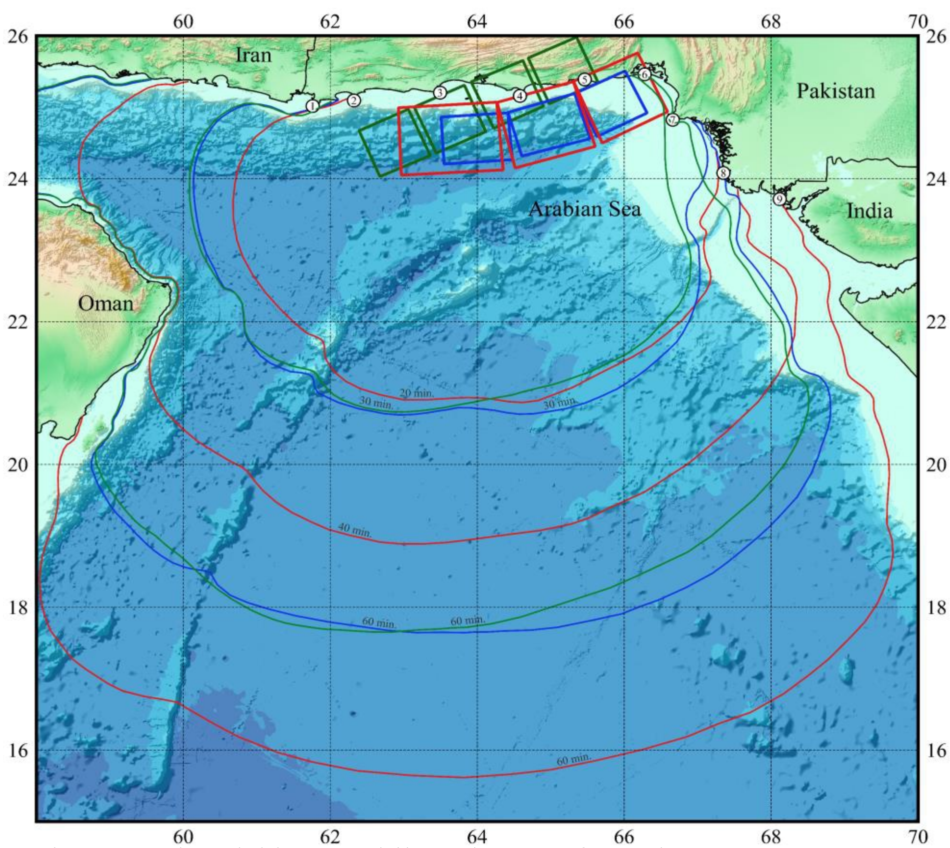

Fig. 6. Red and blue quadrilaterals: FPs from the New-TSM. Green quadrilaterals: FPs from H&S-15. The curves represent tsunami propagation.

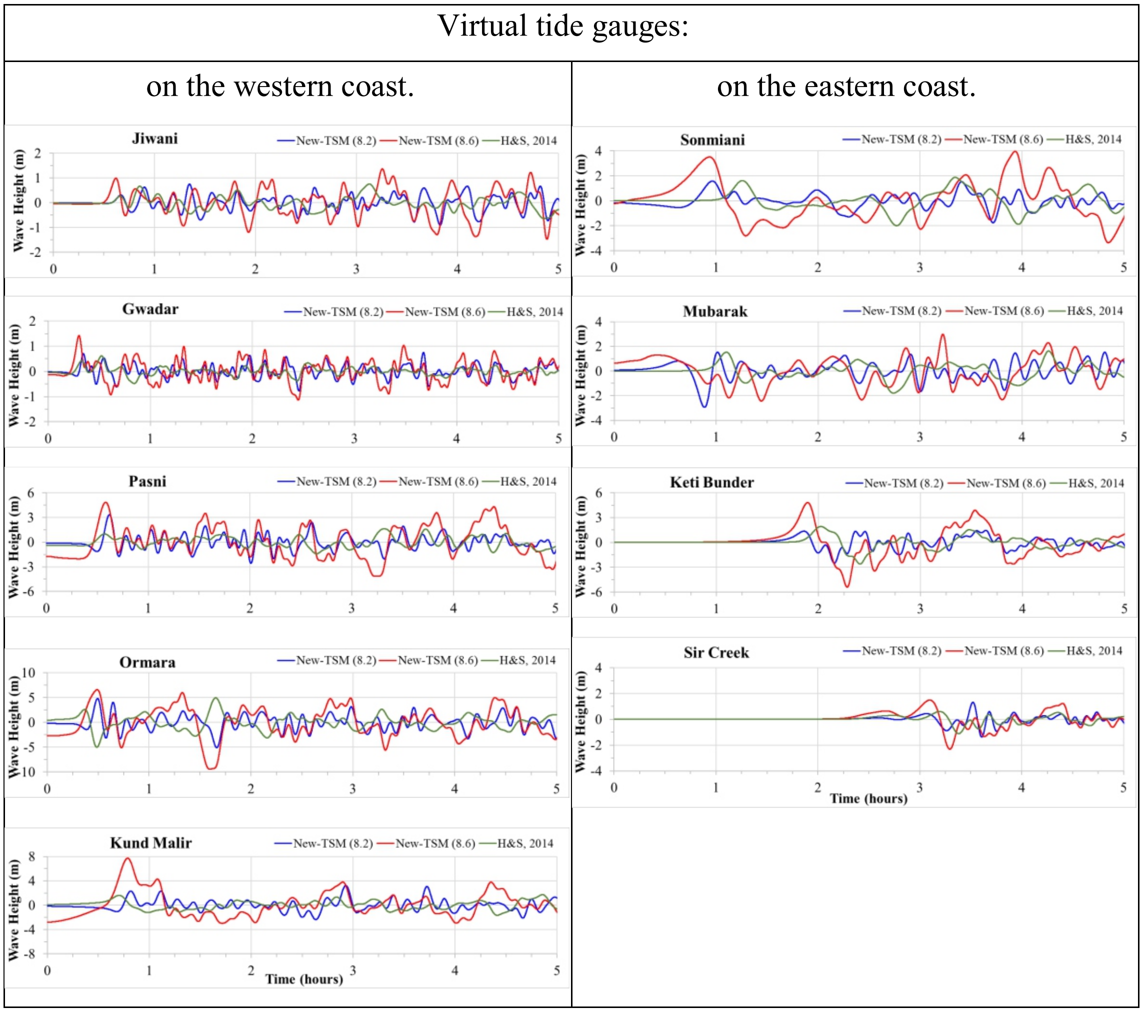

Fig. 7. The tsunami arrival time and wave height from the New-TSM for Mw 8.2 (blue curves) and Mw 8.6 (red curves) earthquakes scenarios, respectively. Green curves represent the waveform from the H&S-15 source model, Mw 8.2 scenario.

In the case of the M_w 8.2 earthquake scenario, Fig. 7 shows that at the eastern coasts, the tsunami waves by the New-TSM (blue curves) arrive (~10 minutes) earlier while at the western coasts, the tsunami waves by the H&S-15 (green curves) arrives 2 to 7 minutes earlier. Therefore, the initial sea-bed displacement (due to Δu along the fault planes) by the New-TSM is closer to the eastern coast (Fig. 6) and the same for the H&S-15 is closer to the western coasts. This results in an earlier arrival of tsunamis at the respective coasts. The first arrival recorded by the tide gauges at Jiwani and Gwadar from both models is simultaneous with identical amplitudes. However, the amplitudes of first waves recorded by the tide gauge at Pasni, Ormara, and Kund Malir by the New-TSM are larger than those by the H&S-15. At Sonmiani and Mubarak the amplitudes of waves from both models are almost the same. At Keti Bunder, the amplitude of H&S-15's model is a little higher than the one determined by the New-TSM. The Sir Creek tide gauge gave a contrary observation to the one at Keti Bunder.

At Jiwani, Sonmiani and Mubarak, the first tsunami wave exhibits a smaller amplitude than those arriving later for the M_w 8.6 earthquake scenario, as depicted in Fig. 7. At tide gauges on the western coast, the tsunami waves simulated by the M_w 8.2 scenarios lag behind that simulated by the M_w 8.6 scenario by ~10 minutes. After the first arrival, the pattern of the following waves is just about the same. Furthermore, the nonstop arrival of tsunami waves can be observed hours after the first tsunami in all earthquake scenarios.

A comparison of the 'first wave's arrival time' (FW time) and the 'highest wave's arrival time' (HW time) is presented in Fig. 8. The

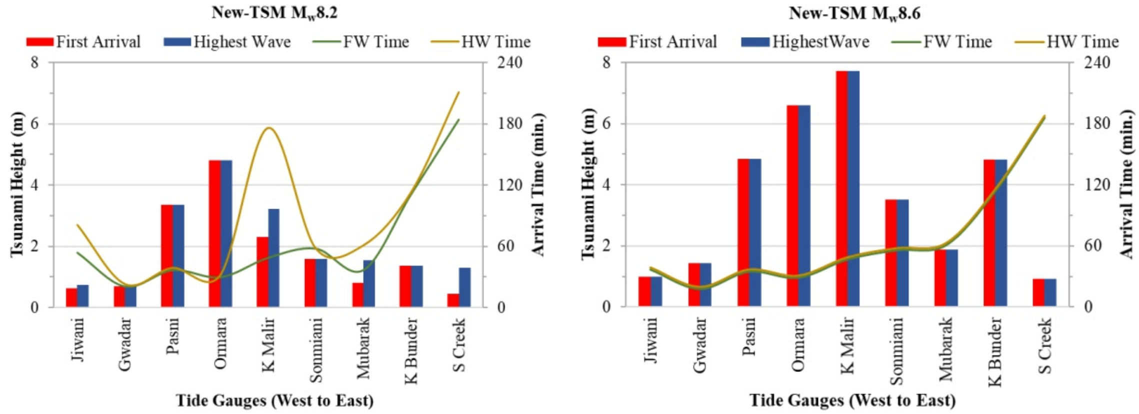

Fig. 8. The first arriving tsunami wave together with the highest tsunami waves. The 8.2 earthquake scenario is shown in left panel whereas 8.6 earthquake scenario is depicted in right panel.

5. Discussion

This study aims to analyze the tsunami hazard by formulating a source model that can fill the gaps in previously developed models for the tsunami simulation in the MSZ. Inadequate tide gauge data, lack of the earthquake source parameters, in addition to the non-availability of an eye-witness account of the 1945 tsunami are some of the foremost difficulties in the formulation of a tsunami source model that can provide its true picture.

The DTHA method is used in this study that relies on detailed and specific inputs such as tsunami source characteristics, bathymetry, and shoreline topography hence providing more accurate and precise results. Fewer simulations are required by the DTHA which saves computational resources, making it a more efficient and cost-effective approach. The DTHA provides straightforward and comprehensible results, in the form of maps and visualizations. The DRR planners, policy-makers, and other stakeholders (who are sometimes non-experts) can easily understand the potential tsunami hazards from these products. Considering these advantages, the DTHA approach is adopted.

The formulation of the New-TSM relies on those features of the MSZ which control the spreading pattern and height of the tsunami. These features include its location, rupture geometry (θ, δ and λ), length and width, focal depth, and displacement. We introduced and applied the novel idea of relating the rupture size of the 1945 earthquake to the total 'area of fault planes' in the formulation of the New-TSM. Analysis of reliable earthquake catalogs is carried out to assign depth to the fault planes. For the hypothetical earthquakes in simulations, the vertical displacement of the seabed is fixed at 11 m by adjusting the moment magnitude, area of the fault planes, and the seismic moment in the scaling law. The whole fault plane does not dislocate with a uniform co-seismic slip. However, for the sake of simplicity, we used the averaged uniform slip.

The positioning of the fault planes and their θ is approximated by 'overlaying' and 'georeferencing' the tectonic maps obtained from eminent research. Some GIS techniques are used by employing the latest software. Three fault planes are seamlessly synchronized with the eastern segment of the MSZ. Earlier studies did not address this aspect, for instance, Heidarzadeh and Satake (2015) considered four fault planes all having identical strike θ. Two out of four fault planes are placed inland not coinciding with the MSZ. Only one fault plane is considered by Zuhair and Alam (2017). The distance between this fault plane and the MSZ is too large. The scientific literature on regional tectonics and precedential research on tsunami simulations are consulted to allocate a suitable value to the dip (δ) and rake (λ) of the fault planes.

Mostly, the previous research on tsunami simulations considered the MSZ as a single segment. Its total length is almost 1000 km. The enormity of the length can lead to overestimations of the maximum credible earthquake giving results that might be beyond the actual. We adopted the theology on the segmentation of the MSZ to avoid such errors.

The eastern section of the MSZ is seismically more active than its western segment. Also, the former is situated nearer and aligns with the coasts of Pakistan. Thus, the eastern MSZ poses a foremost tsunami threat to these coasts. Approximation of the area of the source region of the New-TSM, positioning and alignment of its FPs are all done concerning this segment of the MSZ. The maximum possible earthquake for the eastern MSZ is M_w 8.6 which is used to predict the worst tsunami scenario. For $M_w > 8.6$, either the FPs violate the extent of this segment or overlap each other. Moreover, the cumulative area (length × width) of the fault planes becomes larger as compared to the entire area of the eastern segment of the MSZ. The theory on segmentation of the MSZ limited the maximum earthquake attributed to this zone.

The tsunami waves due to the 1945 earthquake kept hitting the coast continuously for several hours and their amplitudes reached 12 – 15 m. Two standpoints are interpreting these phenomena. Most researchers believe that an underwater landslide, followed by the earthquake, intensified the impacts of this tsunami. The other standpoint is about the trapping of tsunami waves on the continental shelf. These waves continuously hit the coasts for more than a few hours after the first tsunami wave. The shelf has non-uniform width of the entire coasts of Pakistan (Fig. 6). The amplification and non-stop arrival of waves at the coasts is due to their superposition, as these waves got trapped and reverberated on these shelves. The simulation results support the findings of Neetu *et al*. (2011). At Sir Creek, Mubarak, Kund Malir, and Jiwani in the 8.2 magnitude earthquake scenario, higher amplitudes of the waves arriving after the first tsunami are observed (Fig. 8). However, different behavior in the M_w 8.6 earthquake scenario on the continental shelf is demonstrated by the reverberating waves.

Rastgoftar and Soltanpour (2016) claimed that the occurrence of a submarine landslide in the vicinity of Pasni and Ormara amplified the 1945 tsunami and higher waves were observed here as compared to the other coastal towns. Our simulation results yielded higher waves at these sites without the consideration of a submarine landslide. This suggests that the higher waves are due to the closeness of these sites to the epicenter rather than the landslide. Moreover, the analysis of the bathymetry profile revealed the likelihood of landslides along the entire Pakistani coast negating, the idea of limiting the landslide to only these two sites.

The tide gauge at Kund Malir recorded the maximum tsunami amplitude of 7.71 m in the M_w 8.6 earthquake scenario. The tsunami amplitudes from the 8.2 magnitude earthquake scenario are ~ 4.5 m lesser than the amplitudes obtained from the 8.6 magnitude earthquake scenario. Nevertheless, a height of 12 – 15 m is not observed in any simulation. This raises two apprehensions: firstly, whether the cascading effect of the landslide was sufficient to generate a 12 m high tsunami in 1945 which the M_w 8.6 earthquake could not simulate; secondly, whether the reported height of this tsunami is overstated.

The tsunami propagation yielded from the New-TSM and H&S-15's source model for M_w 8.2 (Fig. 6) is similar near the coasts of Oman the reason that the tsunami waves propagated perpendicularly to the strike of the source area in both cases. The strike and location of the fault planes mark a significant gap in the arrival time of tsunami simulated by the New-TSM and the H&S-15 as observed on the eastern Pakistani coasts and the adjacent Indian coasts. The tsunami waves arrived earlier in the case of the New-TSM than in H&S-15's model. The time difference for Sonmiani is 17 minutes, for Mubarak is 28 minutes, and for Keti Bunder is 11 minutes. In case of tsunami prediction, a few minutes are vital for the early warning and the subsequent evacuation. The amplitudes yielded from the New-TSM are higher than H&S-15's model at some parts of the coast. For example, at Pasni, the difference is 2.4 m, at Ormara it is 2.1 m, at Kund Malir it is 0.5 m, and at Sir Creek it is 0.7 m.

In the case of H&S-15's model, a substantial area of the fault planes is situated inland. Contrarily, the fault planes of New.

TSM are completely under the Arabian Sea. The seismic energy produced by the fault planes is transferred to the sea bed. The energy has a direct relationship with the tsunami amplitude. Due to the placement of the fault planes in these cases, the amount of transferred seismic energy is not equal. Thus, H&S-15's model yielded lower tsunami heights as some of their energy could not be transferred to the sea bed.

The tsunami wave simulated by the M_w 8.2 earthquake attacked the coasts a few minutes after those simulated by the M_w 8.6 earthquake (Fig. 7). There are two possible reasons, firstly, the vertical displacement of the seabed is the same in all scenarios (as Δu = 11 m). Consequently, the initial sea-bed displacement is of the same order. Nevertheless, the extent of the sea-bed displacement (which corresponds to the area of the fault planes) is larger for the 8.6 earthquake and closer to the coasts. Hence, the tsunami triggered by this earthquake arrived on the coasts before that generated by the 8.2 magnitude earthquake. Secondly, the velocity 'V' of tsunami waves is given as:

$$x = \sqrt{g(D + A)}, \qquad (3)$$

where $'g'$ represents the gravitational acceleration, $'D'$ stands for the depth of sea, and $'A'$ corresponds to the amplitude of the tsunami wave (Truong, 2012). Velocity would depend only on $'A'$ provided bathymetric conditions remain the same. The tsunami source in both scenarios is the same and both waves traveled through the same bathymetric conditions, nevertheless, the tsunami amplitudes from the M_w 8.6 are higher than those simulated by the M_w 8.2 earthquake scenarios all along the coasts (Fig. 8). Therefore, the tsunami waves simulated by the M_w 8.6 earthquake scenario propagated at a higher velocity. It is established that with the increase in earthquake magnitude in the eastern MSZ, the tsunami arrival time for the adjoining coast gets shorter.

6. Conclusion

- The authors developed the New-TSM to assess the deterministic tsunami hazard for Pakistani coasts. The discrepancies found in previous research are addressed while formulating the New-TSM by considering the geological and seismotectonic characteristics of the MSZ. The location, strike angle, and segmentation of the MSZ rely on GIS techniques. The theory on MSZ segmentation is applied, and the eastern MSZ is identified as a source region in the New-TSM.
- The dimensions of the fault planes in the 8.2 magnitude earthquake scenario are equated to the rupture size of the 1945 earthquake, resulting in a realistic tsunami simulation. Previous studies with large fault planes led to an overestimation of the Mw and affected the subsequent tsunami simulations. The maximum credible earthquake for the eastern segment is estimated to be Mw 8.6 by limiting the size of the fault planes and seismic moment.
- The New-TSM and Heiderzadeh and Satake (2015) models are compared in simulating the tsunami from the Mw 8.2 earthquake, with the latter yielding lower tsunami amplitudes and delayed arrival times. The highest simulated tsunami wave amplitudes are observed at Ormara and Pasni, which tend to refute the hypothesis about the impact of submarine landslides on the 1945 tsunami. Amplified waves kept hitting the coastline persistently until a few hours after the earthquake due to reverberations on the continental shelf.
- Increasing the Mw from 8.2 to 8.6 did not yield ~12 m high tsunami waves as reported in some of the previous studies. Only a 7.71 m high wave is observed as the highest at Kund Malir from the Mw 8.6 scenario. The other notable waves are observed at Ormara (6.61 m high) and Pasni (4.85 m high). These two towns are at the western coast of Pakistan. These are more vulnerable to tsunamis because the tsunami arrived within 29 to 47 minutes. The comparison of the 8.2 and 8.6 magnitude earthquake scenarios in the eastern MSZ proposed that large tsunamigenic earthquakes can trigger faster waves as compared to those generated by relatively smaller earthquakes.

Acknowledgement

The numerical model is provided by

Prof. Takahito Mikami of the Tokyo City University. Without his valuable guidance the tsunami simulations could not be conducted. The authors are thankful to him. The authors are also obliged to two anonymous reviewers who gave valuable suggestions to improve the manuscript.

Authors' Contribution

The main idea of the article is conceived by Babar Ali. The computation related work, including tsunami simulations, preparation of maps, illustrations, figures and tables are performed by him. Moreover, he did the write up of the manuscript.The main concept proposed by Ryo Matsumaru. He supervised the preparation of manuscript including its structure. He also did the proof reading and gave technical review before the submission of the manuscript. Hammad Tariq Janjuhah suggested the literature related to the geology and seismotectonics of the study area. He reviewed and proof read the relevant part of the manuscript.

References

Ambraseys, N.N., Melville, C.P., 1982. A History of Persian Earthquakes. Cambridge University Press, Cambridge, 219 p.

Berninghausen, W.H., 1966. Tsunamis and Seismic Seiches Reported from Regions Adjacent to the Indian Ocean. Bull. of the Seism. Soc. of Am., 56(1), 69–74.

Bilham, R., Lodi, S., Hough, S., Bukhary, S., Khan, A.M., Rafeeqi, S.F.A., 2007. Seismic hazard in Karachi, Pakistan: uncertain past, uncertain future. Seis. Res. Lett., 78, 601–3.

BODC, 1997. British Oceanographic Data Centre – The Centenary Edition of the GEBCO Digital Atlas (download.gebco.net), Liverpool, UK.

Bonilla, M.G., Mark, R.K., Lienkaemper, J.J., 1984. Statistical relation among earthquake magnitude, surface rupture and surface fault displacement. Bul. Seism. Soc. Amer., 74(6), 2379-2411.

Burg, J.P., 2018. Geology of the onshore Makran accretionary wedge: Synthesis and tectonic interpretation. Earth-Science Reviews 185, 1210-1231.

Byrne, D.E., Sykes, L.R., Davis, D.M., 1992. Great thrust earthquakes and aseismic slip along the plate boundary of the Makran subduction zone. Journal of Geophysical Research, 97. doi: 10.1029/91JB02165. ISSN: 0148-0227.

Farhoudi, G., Karig, D.E., 1977. Makran of Iran and Pakistan as an Active Arc System, Geology, 5, 664–668.

Gutenberg, B., Richter, C.F., 1954. Seismicity of the Earth and Associated Phenomena, Princeton Univ. Press, Princeton, 310 p.

Hanks, T.C., Kanamori, H., 1979. A Moment Magnitude Scale. Journal of Geophysical Research, 84(B5), 2348–2350. doi: 10.1029/JB084iB05p02348.

Harbitz, C. B., Lovholt, F., and Bungum, H., 2014. Submarine landslide tsunamis: how extreme and how likely? Nat. Hazards 72 (3), pp. 1341–1374.

HCP, 2008. Helmholtz Centre Potsdam - GFZ German Research Centre for Geosciences and Gempa GmbH. The SeisComP Seismological Software Package. GFZ Data Services.

Heck, N.H., 1947. List of Seismic Sea waves, Bull. Seismol. Soc. Am. 37(4), 269–286.

Heidarzadeh, M., Pirooz, M.D., Zaker, N.H., Yalciner, A.C., Mokhtari, M., Esmaeily, A., 2008. Historical tsunami in the Makran subduction zone off the southern coasts of Iran and Pakistan and results of numerical modeling, Ocean Eng., 35(8 - 9), 774–786.

Heidarzadeh, M., Pirooz, M.D., Zaker, N.H., Yalciner, A.C., 2009. Preliminary Estimation of the Tsunami Hazards Associated with the Makran Subduction Zone at the Northwestern Indian Ocean, Nat. Hazards, 48(2), 229–243.

Heidarzadeh, M., Satake, K., 2015. New Insights into the Source of the Makran Tsunami of 27 November 1945 from Tsunami Waveforms and Coastal Deformation Data. Pure and Appl. Geophys., doi:10.1007/s00024-014-0948-y.

Hoffmann, G., Rupprechter, N., Albalushi, N., Grutzner, C., Reicherter, K., 2013. The Impact of the 1945 Makran Tsunami along the Coastlines of the Arabian Sea (Northern Indian Ocean) – a review, Z. Geomorphologie 57(4), 257–277.

Jaiswal, R.K., Singh, A.P., Rastogi, B. K., 2009. Simulation of the Arabian Sea Tsunami Propagation Generated due to 1945

Makran Earthquake and its Effect on Western Parts of Gujarat (India), Nat. Hazards, 48(2), 245–258.

Kakar, D.M., Naeem, G., Usman, A., Hasan, H., Lohdi, H.A., Srinivasalu, S., Andrade, V., Rajendran, C.P., Naderi, A., Beni, Hamzeh, M.A., Hoffmann, G., Al-Balushi, N., Gale, N., Kodijat, A.M., Fritz, H.M., Atwater, B.F., 2014. Elders Recall an Earlier Tsunami on Indian Ocean Shores. Eos, 95(51), 485 – 486.

Kazmi, A.H., Jan, M.Q.,1997. Geology & Tectonics of Pakistan. Graphic Pub., Karachi.

Khan, A.A., 1999. Offshore Geology of Pakistan and Non-living Resource Prospects. Pakistan Journal of Marine Sciences, 8(1), 81–97.

Kukowski, N., Schillhorn, T., Huhn, K., Rad, U., Husend, S., Flueh, E.R., 2001. Morphotectonics and Mechanics of the Central Makran Accretionary Wedge off Pakistan. Marine Geology, 173(1-4), 1-19.

Lorito S., Tiberti M.M., Basili R., Piatanesi A., Valensise G., 2008. Earthquake-generated tsunamis in the Mediterranean Sea: scenarios of potential threats to southern Italy. J Geophys Res Solid Earth.

Lovholt, F., Bungum, H., Harbitz, C. B., Glimsdal, S., Lindholm, C. D., Pedersen, G., 2006. Earthquake related tsunami hazard along the western coast of Thailand, Nat. Hazards Earth Syst. Sci., 6, pp. 979–997.

Mansinha, L., Smylie, D.E., 1971. The Displacement Fields of Inclined Faults. Bulletin of the Seismological Society of America, 61(5), 1433-1440.

Mikami, T., Tomoya, S., Miguel, E., Koichiro, O., Jun, S., Takayuki, S., Hendra, A., Teguh, W., 2014. Tsunami Vulnerability Evaluation in the Mentawai Islands Based on the Field Survey of the 2010 Tsunami. Nat. Hazards, 71, 851–870.

Musson, R., 2009. Subduction in the Western Makran: The Historian's Contribution. J. Geol. Soc., 166, 387–391. doi.org/10.1144/0016-76492008-119.

Neetu, S., Suresh, I., Shankar, R., Nagarajan, B., Sharma, R., Shenoi, S.S.C., Unnikrishnan, A.S., Sundar, D., 2011. Trapped Waves of the 27 November 1945 Makran Tsunami: Observations and Numerical Modeling, Natural Hazards, 59(3), 1609–1618.

Okal, E.A., Fritz, H., Hamzeh, M., Ghase, J., 2015. Field Survey of the 1945 Makran and 2004 Indian Ocean Tsunamis in Baluchistan, Iran. Pure Appl. Geophys. 172, 3343-3356.

Omira, R., M. A. Baptista, F. Leone, L. Matias, S. Mellas, B. Zourarah, J. M. Miranda, F. Carrilho, and Cherel, J.P., 2013. Performance of coastal sea-defense infrastructure at El Jadida (Morocco) against tsunami threat: lessons learned from the Japanese 11 March 2011 tsunami. Nat. Hazards Earth Syst. Sci., 13, 1779–1794.

W.D., Alt, J.N., Cluff, L.S., Plafker, G., 1979. Evidence for the Recurrence of Large-magnitude Earthquakes along the Makran coast of Iran and Pakistan, Tectonophysics, 52(1), 533–547.

Pararas-Carayannis, G., 2006. The potential for tsunami generation along the Makran Subduction Zone in the Northern Arabian Sea. Case study: the earthquake and tsunami of November 28, 1945. Science of Tsunami Hazard, 24(5), 358–384.

Quittmeyer, R.C., Jacob, K.H., 1979. Historical and Modem Seismicity of Pakistan, Afghanistan, Northwestern India, and Southeastern Iran. BSSA, 69(3), 773–823.

Rajendran, C.P., Ramana, M.V., Reddy, N.T., Rajendran, K., 2008. Hazard Implications of the Late Arrival of the 1945 Makran Tsunami. Current Science, 95(12), 1739-1743.

Rajendran, C.P., Rajendran, K., Shah-Hosseini, M., Beni, A.N., Nautiyal, C.M., Andrews, R., 2012. The Hazard Potential of the Western Segment of the Makran Subduction Zone, Northern Arabian Sea. Nat. Hazards, 65, 219–239.

Rastgoftar, E., Soltanpour, M., 2016. Study and Numerical Modeling of 1945 Makran Tsunami due to a Probable Submarine Landslide. Nat. Hazards, 83, 929–945.

Rehman, K., Jadoon, T., Hussain, M., Ahmad, Z., Ali, A., Ahmed, S., 2015. Tsunamigenic Analysis in and around Makran. Journ. of Earth. Engg, 19(2), 332-355.

Rastogi, B.K., Jaiswal, R.K., 2006. A Catalog of Tsunamis in the Indian Ocean, Science of Tsunami Hazards, 25(3), 128-142.

Shah-Hosseini, M., Morhange, C., Beni, N.A., Marriner, N., Lahijani, H., Hamzeh, M., and Sabatier, F., 2011. Coastal Boulders as Evidence for High-Energy Waves on the Iranian coast of Makran, Marine Geology, 290(1), 17–28.

Snead, R.E., 1966. Recent morphological changes along the coast of west Pakistan. Annals of the Association of American Geographers 57 (3), 550–565.

Solangi, S.H., Adeel, N., Shabeer, A., Mian, M., 2019. Morphologic features continental shelf margin: Examples from Pakistan offshore. Geodesy & Geodynamics, 10, 77-91.

Tinti. S., Armigliato. A., 2003. The use of scenarios to evaluate the tsunami impact in southern Italy. Mar. Geol. 199(3), 221–243.

Tinti S., Armigliato A., Pagnoni G., Zaniboni F., 2005. Scenarios of giant tsunamis of tectonic origin in the Mediterranean. ISET J Earthquake Technol 42(4), 171–188.

Truong, H.V.P., 2012. Wave-Propagation Velocity, Tsunami Speed, Amplitudes, Dynamic Water-Attenuation Factors, 15th WCEE, Lisbon, Portugal.

Zuhair, M., Alam, S., 2017. Tsunami Impacts on Nuclear Power Plants along Western Coast of India Due to a Great Makran Earthquake: A Numerical Simulation Approach. International Journal of Geosciences, 8, 1417-1426. doi.org/10.4236/ijg.2017.812083.